

Cite as: J. Wang *et al.*, *Science* 10.1126/science.aar7053 (2018).

Multidimensional quantum entanglement with large-scale integrated optics

Jianwei Wang,^{1,2*}† Stefano Paesani,^{1*} Yunhong Ding,^{3,4**†} Raffaele Santagati,¹ Paul Skrzypczyk,⁵ Alexia Salavrakos,⁶ Jordi Tura,⁷ Remigiusz Augusiak,⁸ Laura Mančinska,⁹ Davide Bacco,^{3,4} Damien Bonneau,¹ Joshua W. Silverstone,¹ Qihuang Gong,² Antonio Acín,^{6,10} Karsten Rottwitt,^{3,4} Leif K. Oxenløwe,^{3,4} Jeremy L. O'Brien,¹ Anthony Laing,^{1†} Mark G. Thompson^{1†}

¹Quantum Engineering Technology Labs, H. H. Wills Physics Laboratory and Department of Electrical and Electronic Engineering, University of Bristol, Bristol BS8 1FD, UK.

²State Key Laboratory for Mesoscopic Physics, School of Physics, Collaborative Innovation Center of Quantum Matter, Peking University, Beijing 100871, China.

³Department of Photonics Engineering, Technical University of Denmark, 2800 Kgs. Lyngby, Denmark. ⁴Center for Silicon Photonics for Optical Communication, Technical University of Denmark, 2800 Kgs. Lyngby, Denmark. ⁵H. H. Wills Physics Laboratory, University of Bristol, Bristol BS8 1TL, UK. ⁶Institut de Ciències Fotoniques, Barcelona Institute of Science and Technology, 08860 Castelldefels, Barcelona, Spain. ⁷Max-Planck-Institut für Quantenoptik, 85748 Garching, Germany. ⁸Center for Theoretical Physics, Polish Academy of Sciences, 02-668 Warsaw, Poland. ⁹QMATH, Department of Mathematical Sciences, University of Copenhagen, 2100 Copenhagen Ø, Denmark.

¹⁰Institució Catalana de Recerca i Estudis Avançats, 08010 Barcelona, Spain.

*These authors contributed equally to this work.

†Corresponding author. Email: jianwei.wang@bristol.ac.uk (J.W.); yudin@fotonik.dtu.dk (Y.D.); anthony.laing@bristol.ac.uk (A.L.); mark.thompson@bristol.ac.uk (M.G.T.)

The ability to control multidimensional quantum systems is key for the investigation of fundamental science and for the development of advanced quantum technologies. We demonstrate a multidimensional integrated quantum photonic platform able to generate, control and analyze high-dimensional entanglement. A programmable bipartite entangled system is realized with dimension up to 15×15 on a large-scale silicon-photonics quantum circuit. The device integrates more than 550 photonic components on a single chip, including 16 identical photon-pair sources. We verify the high precision, generality and controllability of our multidimensional technology, and further exploit these abilities to demonstrate key quantum applications experimentally unexplored before, such as quantum randomness expansion and self-testing on multidimensional states. Our work provides an experimental platform for the development of multidimensional quantum technologies.

As a generalization of two-level quantum systems (qubits), multidimensional quantum systems (qudits) exhibit distinct quantum properties and can offer improvements in particular applications. For example, qudit systems allow higher capacity and noise robustness in quantum communications (1–3), can be used to strengthen the violations of generalized Bell and Einstein-Podolsky-Rosen (EPR) steering inequalities (4–6), provide richer resources for quantum simulation (7, 8), and offer higher efficiency and flexibility in quantum computing (9, 10). Moreover, encoding and processing qudits can represent a more viable route to larger Hilbert spaces. These advantages motivate the development of multidimensional quantum technologies in a variety of systems, such as photons (11, 12), superconductors (8, 13), and atomic systems (14, 15). While complex interaction engineering and control sequences are required to encode and manipulate superconducting and atomic qudits, photons represent a promising platform able to naturally encode and process qudits in various degrees of freedom, e.g., orbital angular momentum (OAM) (11, 12), temporal modes (3, 16), and frequency (17, 18). Previous work on qudits includes realizations of complex entanglement (19), entanglement in ultra-

high dimension (20), and practical applications in quantum communication (1–3) and computing (7–9). However, these approaches present limitations in terms of controllability, precision and universality, which represent bottlenecks for further developments of multidimensional technologies. For example, the arbitrary generation of high-dimensional entanglement is a key experimental challenge, typically relying on complex bulk-optical networks and post-selection schemes (12, 16–18). In general, these approaches lack the ability to perform arbitrary multidimensional unitary operations with high fidelity (16, 19), an important factor in quantum information tasks. Integrated microring resonators able to emit multidimensional OAM (21) and frequency (18) states have been reported, but these present limited fidelity and difficulties for on-chip state control and analysis, thus not fully exploiting the high precision, scalability and programmability of integrated optics.

We report a multidimensional integrated quantum photonic device that is able to generate, manipulate and measure multidimensional entanglement fully on-chip with unprecedented precision, controllability and universality. Path-encoded qudits are obtained having each photon exists

over d spatial modes simultaneously, and entanglement is produced by a coherent and controllable excitation of an array of d identical photon-pair sources. Our device allows the generation of multidimensional entangled states with an arbitrary degree of entanglement. Universal operations on path-encoded qudits are possible in linear-optics for any dimension (22, 23), and our device performs arbitrary multidimensional projective measurements with high fidelity. The capabilities achieved allow us to demonstrate high-quality multidimensional quantum correlations, verified by generalized Bell and EPR steering violations, and to implement unexplored multidimensional quantum information protocols.

Large-scale integrated quantum photonic circuit

Entangled path-encoded qubits can be generated by coherently pumping two spontaneous parametric down conversion (24) or spontaneous four-wave mixing (SFWM) photon-pair sources (25). The approach can be generalized to qudits via the generation of photons entangled over d spatial modes by coherently pumping d sources (24). However, scaling this approach to high dimensions has been challenging due to the need of a stable and scalable technology able to coherently embed large arrays of identical photon sources and to precisely control qudit states in large optical interferometers.

Silicon quantum photonics, offering intrinsic stability (26), high precision (27) and dense integration (28), can provide a natural solution. We devise a large-scale silicon quantum photonic circuit to implement the scheme (Fig. 1A). A total of 16 SFWM sources are coherently pumped, generating a photon-pair in a superposition across the array. As both the photons must originate from the same source, the bipartite state created is $\sum_{k=0}^{d-1} c_k |1\rangle_{i,k} |1\rangle_{s,k}$ where $|1\rangle_{i,k}$ ($|1\rangle_{s,k}$) indicates the Fock state of the idler (signal) photon being in its k -th spatial mode and c_k represents the complex amplitude in each mode (with $\sum |c_k|^2 = 1$). The mapping between the Fock state of each photon and the logical state is the following: we say that the qudit state is $|k\rangle$ ($k = 0, \dots, d - 1$) if the associated photon is in its k -th optical mode. This yields a multidimensional entangled state of the form:

$$|\psi\rangle_d = \sum_{k=0}^{d-1} c_k |k\rangle_i |k\rangle_s \quad (1)$$

where the coefficients c_k can be arbitrarily chosen by controlling the pump distribution over the d sources and the relative phase on each mode. This is achieved using a network of Mach-Zehnder interferometers (MZIs) at the input and phase-shifters on each mode. In particular, maximally

entangled states $|\psi_d^+\rangle = \sum_{k=0}^{d-1} |k\rangle_i |k\rangle_s / \sqrt{d}$ can be obtained with a uniform excitation of the sources. The two non-degenerate photons are deterministically separated using asymmetric MZI filters and routed by a network of waveguide crossings, grouping the signal photon into the top modes and the idler photon into the bottom ones (see Fig. 1A). We can then locally manipulate and measure the state of each qudit. Linear-optical circuits enable the implementation of any local unitary transformation \hat{U}_d in dimension d (22, 23). A triangular network of MZIs and phase-shifters is used, which allows us to perform arbitrary local projective measurements, and two detectors are used to measure the outcomes. In this scheme, the measurement outcomes on a specific basis are collected one by one by rotating the qudits reference frame and using one detector per photon. The collection of the d^2 outcomes thus requires d^2 detections in total. For more general implementations, the simultaneous collection of all the outcomes can be achieved via universal qudit operations (23) and the detection of each photon on all the output modes with $2d$ detectors (inset of Fig. 1A). For more details on the device and the experimental setup see (29).

The 16 photon-pair sources are designed to be identical. Two-photon reversed Hong-Ou-Mandel (RHOM) interference is used to verify their performance, where the fringe visibility gives an estimate of the sources' indistinguishability (26). RHOM interference is tested between all the possible pairs of the 16 sources, performing $\binom{16}{2} = 120$ quantum interference experiments and evaluating the corresponding visibilities. The pair of sources used for each interference experiment is selected each time by reconfiguring the interferometric network. Approximately a rate of 2kHz photon-pair coincidences was observed in typical measurement conditions, from which accidentals were subtracted. For the measured visibilities (Fig. 1D), in all cases we obtained a visibility > 0.90 , and more than 80% cases presented > 0.98 visibility. These results show a state-of-the-art degree of source indistinguishability in all 120 RHOM experiments, leading to the generation of high quality entangled qudit states.

Each of the MZIs and phase-shifters can be rapidly reconfigured (kHz rate) with high precision (26, 28). The quality of the qudit projectors is characterized by the classical statistical fidelity, which quantifies the output distribution obtained preparing and measuring a qudit on a fixed basis. We measured the fidelity of projectors in dimension $d = 2$ to 16 in both the computational basis $\hat{Z} = |k\rangle\langle k|$, and in the Fourier-transform basis $\hat{F} = |\ell\rangle\langle \ell|$, where $|\ell\rangle = \sum_{k=0}^{d-1} \exp(2\pi i k \ell / d) |k\rangle / \sqrt{d}$ and $k, \ell = 0, \dots, d - 1$ (Fig. 1E). We observe for $d = 8$ fidelities of

98% in the \hat{Z} -basis and 97% in the \hat{F} -basis, while for $d = 16$ fidelities of 97% in the \hat{Z} -basis and 85% in the \hat{F} -basis (29). The residual imperfections are mainly due to thermal cross-talk between phase-shifters (higher in the \hat{F} -basis), which can be mitigated using optimized designs for the heaters (28) or ad hoc characterization techniques (23).

Due to a fabrication imperfection in the routing circuit one of the modes (triangle label in Fig. 1A) for the idler photon presents an additional 10 dB loss. For simplicity we exclude this lossy mode in the rest of our experiments, and study multidimensional entanglement for dimension up to 15.

Figure 1B represents the experiment in the standard framework for bipartite correlation. The correlations between two parties Alice (A) and Bob (B), here identified by the signal and idler photon respectively, are quantified by joint probabilities $p(ab|xy) = \text{Tr}[\hat{\rho}_d(\hat{M}_{a|x} \otimes \hat{M}_{b|y})]$, where $\hat{\rho}_d$ is the shared d -dimensional state, $x, y \in \{1, \dots, m\}$ represent the m measurement settings chosen by Alice and Bob, and $a, b \in \{0, \dots, d - 1\}$ label the possible outcomes with associated measurement operators $\hat{M}_{a|x}$ and $\hat{M}_{b|y}$. The joint probabilities for each measurement are calculated by normalizing the coincidence counts over all the d^2 outcomes in a given basis.

Quantum state tomographies

Quantum state tomography (QST) allows us to estimate the full state of a quantum system, providing an important diagnostic tool. In general, performing a complete tomography is an expensive task both in terms of the number of measurements and the computational time to reconstruct the density matrix from the data. For these reasons complete QST on entangled qudits states has been achieved only up to 8-dimensional systems (30). In order to perform the tomographic reconstructions of larger entangled states, we use quantum compressed sensing techniques. Inspired by advanced classical methods for data analysis, these techniques reduce the experimental cost for state reconstruction (31), are general for density matrices of arbitrary dimension (32), and have been experimentally demonstrated to characterize complex quantum systems (32, 33). Compressed sensing QST was implemented to reconstruct bipartite entangled states with local dimension up to $d = 12$. Fidelities with ideal states $|\psi_d^+\rangle$ are reported in Fig. 2A. For dimensions $d = 4, 8$ and 12 we plot the reconstructed density matrices, with fidelities of 96%, 87%, and 81%, respectively (Fig. 2). These results show an improvement of the quality for multidimensional entanglement (18, 30). More details are

reported in (29).

Certification of system dimensionality

The dimension of a quantum system quantifies its ability to store information and represents a key resource for quantum applications. Device-independent (DI) dimension witnesses enable us to lower bound the dimension of a quantum system solely from the observed statistics, i.e., correlation probabilities $p(ab|xy)$, making no prior assumptions on the experimental apparatus (see e.g., (34, 35)). Here, we adopt the approach of (35) to verify the local dimension of entangled states in a DI way in the context where shared randomness is not a free resource. The lower bound on the system dimension is given by $\lceil \mathcal{D}(p) \rceil$, where $\mathcal{D}(p)$ is a nonlinear function of the correlations, and $\lceil \cdot \rceil$ indicates the least integer $\geq \varepsilon$. While with d we indicate the local dimension of the qudit encoded in d modes, $\lceil \mathcal{D}(p) \rceil$ represents the certified dimension of the quantum system, that is the minimum dimension required to describe the observed correlations. We adopt two different DI measurement scenarios, with experimental results shown in Fig. 3A. In scenario I, we calculate the bound from the measured (partial) correlations for the Magic Square and Pentagon games (36) (Fig. 3B). For example, to certify 8×8 entangled states, locally equivalent to a 3-qubit system, we perform a \hat{Z} -basis measurement on Alice's system, while on Bob's system we use the \hat{Z} -basis and the one which simultaneously diagonalizes the commuting operators ZZZ, ZXX, XZX , and XXZ (see lines L3 and L5 in Fig. 3B respectively). In the absence of noise we would achieve $\mathcal{D} = 8$. Using the measured correlations we obtain $\mathcal{D}(p_8^I) \geq 7.22 \pm 0.05$ which yields the optimal lower bound $\lceil \mathcal{D}(p_8^I) \rceil = 8$. In scenario II, we compute $\mathcal{D}(p_d^{II})$ for correlations p_d^{II} obtained by performing \hat{Z} -basis measurements on both sides of the maximally entangled state of local dimension d . We expect less experimental noise in this scenario (see Fig. 1D). As shown in Fig. 3A, the experimentally observed correlations p_d^{II} yield $\lceil \mathcal{D}(p_d^{II}) \rceil = d$ for all $d \leq 14$, certifying the correct dimensions. Further details can be found in (29).

Multidimensional Bell correlations and state self-testing

Bell inequalities enable to experimentally study quantum non-locality, which indicates the presence of correlations incompatible with local-hidden variables (LHV) theories.

Non-locality can be demonstrated by the violation of Bell inequalities of the form $S_d \leq C_d$, where the expression S_d is a linear function of the joint probabilities, and C_d is the classical bound for LHV models. Although our implementation does not represent a rigorous and loophole-free test of non-locality, Bell inequalities are here used as an experimental tool to benchmark the quality of the multidimensional entanglement and to investigate possible future applications. We study two types of generalized Bell-type inequalities for d -dimensional bipartite systems: the SATWAP inequalities (Salavrakos-Augusiak-Tura-Wittek-Acin-Pironio), recently introduced in (6), and the standard CGLMP inequalities (Collins-Gisin-Linden-Massar-Popescu) (5). In contrast to CGLMP inequalities, SATWAP inequalities are explicitly tailored to obtain a maximal violation for maximally entangled qudit states. Here we test the 2-input version of the SATWAP inequalities by measuring the joint probabilities to obtain the quantity

$$\tilde{I}_d = \sum_{i=1}^2 \sum_{l=1}^{d-1} \langle A_i' \bar{B}_i' \rangle \quad (2)$$

where the $2(d - 1)$ values $\langle A_i' \bar{B}_i' \rangle$ represent generalized Bell correlators, whose explicit form is given in (29). The Bell inequality here is given by $\tilde{I}_d \leq C_d$, where the bound for classical LHV models is $C_d = [3\cot(\pi/4d) - \cot(3\pi/4d)]/2 - 2$. The maximum value of \tilde{I} obtainable with quantum states (Tsirelson bound) is known analytically for arbitrary dimensions and is given by $\tilde{I}_d \leq Q_d = 2d - 2$. This maximal violation is achieved with maximally entangled states (6).

In Fig. 4A we show the experimental values of the generalized correlators $\text{Re}[\langle A_i' \bar{B}_i' \rangle]$. The correlation measurements are performed in the Fourier bases provided in (29). Figure 4B shows the obtained values of \tilde{I}_d for dimensions 2 to 8, together with the analytical quantum and classical bounds. In all cases the classical bound is violated. In particular in dimensions 2–4 a strong violation is observed, closely approaching the Tsirelson bound Q_d .

We report in Table 1 the experimental values for the CGLMP inequalities. Also for CGLMP, strong violations of LHV models are observed. As an example, for $d = 4$ we observe $S_4 = 2.867 \pm 0.014$, which violates the classical bound (i.e., $C_d = 2$ for CGLMP inequalities) by 61.9σ , and is higher than the maximal value achievable by 2-dimensional quantum systems ($S_2 = 2\sqrt{2}$) by 2.8σ , indicating stronger quantumness for higher dimensions.

The near-optimal Bell violations enable the self-testing

of multidimensional entangled states. The task of self-testing represents the DI characterization of quantum devices by a classical user, based solely on the observed Bell correlations (37, 38), and thus does not require making any assumption about the devices being tested, which is desirable for practical quantum applications. In more details, if the maximal violation of a Bell inequality can only be achieved by a unique quantum state and set of measurements (up to local isometries), a near-optimal violation enables to characterize the experimental device. In (6) it was shown that the SATWAP inequality can be used to self-test the maximally entangled state of two qutrits $|\Psi_3^+\rangle$; in particular, employing a numerical approach from (39), a lower bound on the state fidelity can be obtained from the measured value of \tilde{I}_3 . In (29) we generalize it also for arbitrary qutrit states of the form $|00\rangle + \gamma|11\rangle + |22\rangle$ (up to normalization). In Fig. 4C we report the experimental self-tested lower bounds on the fidelities for different values of $\gamma = 1, 0.9$, and $(\sqrt{11} - \sqrt{3})/2 \approx 0.792$. This is possible by exploiting the capability of the device to generate multidimensional states with tunable entanglement. In particular, $\gamma = 1$ indicates $|\Psi_3^+\rangle$ and $\gamma = (\sqrt{11} - \sqrt{3})/2$ represents the state that maximally violates the CGLMP inequality (39). We experimentally achieve self-tested lower bounds on the fidelities of 79.9%, 83.2% and 68.0% respectively for the three states. We remark that the certification of high fidelities in a self-testing context is only achievable in the presence of near-ideal experimental correlations. The measured self-tested fidelities are comparable with the reported values obtained from full tomographies in other experimental approaches (18, 30). Although our device provides high violations also for dimensions higher than 3, it remains an open problem whether the approach based upon SATWAP inequalities can be generalized to self-test states in arbitrary dimension (6).

Multidimensional randomness expansion

Randomness is a key resource in many practical applications. Generating certified randomness is however a notoriously difficult problem. Quantum theory, being fundamentally nondeterministic, provides a natural solution. The probabilistic nature of measurements forms the basis of quantum random number generators (40). Remarkably, quantum theory can go one step further and allows a stronger form of certified randomness: measurement statistics which exhibit non-local correlations are necessarily uncertain and contain randomness. Crucially this remains true even if some or all of the experimental apparatuses used to generate the non-local correlations are uncharacterized or untrusted (41). That is, the measurement statistics are ran-

dom not only for the user of the devices but also for any other party who may have additional knowledge about the devices, such as a potential eavesdropper.

The two scenarios considered here are: (i) Randomness certified by Bell inequality violations, where two untrusted measuring apparatuses are used to generate randomness, providing a fully DI certification (41); (ii) Randomness certified by EPR steering inequality violations, where one trusted and one untrusted measuring apparatuses are used, with randomness generated from the untrusted device, providing a one-sided DI (1SDI) certification (42).

The protocol in either case consists of performing n runs of a Bell or steering test, using a small seed of randomness to choose the measurement settings in each run. The violation of the corresponding Bell or steering inequality is then estimated from the raw data. The randomness of the string \mathbf{s} of measurement outcomes of the untrusted apparatuses is then lower bounded as a function of the observed violation. Since an initial seed of randomness is necessary, this process achieves randomness expansion as new private randomness is generated in the process. The randomness of the string \mathbf{s} is quantified in terms of min-entropy $H_{\min} = -\log_2 P_g$, where P_g is the predictability of \mathbf{s} , i.e., the probability it can be correctly guessed.

To study DI randomness expansion, we use violations of the above SATWAP Bell inequalities, while in the 1SDI case we use violations of the EPR steering inequality (29)

$$\beta_d = \sum_{\substack{a=b \\ x=y}} p(a|x) \text{Tr} \left[\hat{M}_{b|y} \hat{\rho}_{a|x} \right] \leq 1 + 1/\sqrt{d} \quad (3)$$

Here $p(a|x)$ are the probabilities of Alice's uncharacterized measurements; $\hat{M}_{k|0} = |k\rangle\langle k|$, $\hat{M}_{\ell|1} = |\ell\rangle\langle -\ell|$ are the characterized measurements of Bob, with $|k\rangle$ corresponding to the \hat{Z} -basis and $|\ell\rangle$ to the \hat{F} -basis, defined above; $\hat{\rho}_{a|x}$ indicates the reduced state for Bob when the measurement x is performed on Alice and outcome a is obtained. Quantum states can violate this inequality and maximally achieve $\beta_d = 2$. Figure 5A reports the experimentally measured values of β_d up to dimension 15, which display violations of the local bound in all dimensions. We note that this provides a 1SDI certification of the presence of bipartite multidimensional entanglement between Alice and Bob in all cases (4).

In the DI setting, the measuring apparatuses of Alice and Bob are both untrusted, and the string of outcomes $\mathbf{s} = (\mathbf{a}, \mathbf{b})$, where \mathbf{a} (\mathbf{b}) is the list of data collected by Alice (Bob). In the 1SDI setting the measuring apparatus of Alice is untrusted, and the string of outcomes is $\mathbf{s} = \mathbf{a}$. Details of how randomness is certified, as well as the maximal theoretical

amount of randomness that can be certified in each case are provided in (29). A particularly demanding task is the efficient generation of randomness – to generate more than 1 bit of randomness per experimental run, i.e., to achieve $H_{\min} > n$. For qubits, this is only possible using non-projective measurements (with more than 2 outcomes) (43) or with sequences of measurements (44). In contrast, multidimensional entangled states provide a natural route based upon projective measurements.

In Figs. 4B and 5A the minimum values of \bar{I}_d and β_d above which more than one bit of randomness per run is certified in the DI or 1SDI setting, are shown as a function of dimension (yellow regions). The randomness associated with the Bell violations shown in Fig. 4A, are reported in Fig. 5C. Efficiency $H_{\min}/n > 1$ is achieved for $d = 3$ and 4. The largest amount of randomness per run is obtained for $d = 4$, where $H_{\min}/n = 1.82 \pm 0.35$ random bits. The experimentally measured values of β_d are shown in Fig. 5A, and the associated randomness is reported in Fig. 5B. Here efficiency $H_{\min}/n > 1$ is preserved for the range $4 \leq d \leq 14$, indicating, as expected, stronger robustness in the 1SDI case.

Conclusion

We have shown how silicon-photonics quantum technologies have reached the maturity level which enables fully on-chip generation, manipulation and analysis of multidimensional quantum systems. The achieved complexity of our integrated device represents a significant step forward for large-scale quantum photonic technologies. We remark that in the experimental tests performed here the detection and locality loopholes were not closed, which was not an immediate goal of this work. However, the results demonstrate the unprecedented capabilities of multidimensional integrated quantum photonics which will enable a wide range of practical applications. For example, high-rate device-independent randomness generators can be realized harnessing the abilities of efficient randomness expansion shown here and high-speed on-chip state manipulation. As a single chip proof-of-principle demonstration of quantum key distribution, we report in (29) that Alice and Bob can share high-rate secure keys enabled by the high-fidelity control and analysis of the entangled qudits. Together with developed techniques for the phase coherent chip-to-chip qudits transmission, e.g., via a multi-core optical fiber (45), encoding in other degrees of freedom in free space (46), and exploiting reference-frame-independent schemes (47), our integrated platform can allow the development of high-dimensional quantum communications. All these possible applications can benefit from the monolithic integration of high-performance sources, universal operations and detectors (26). Moreover, the scalability of silicon quantum photonics can further increase system dimensionality, and allow

the coherent control of multiple photons entangled over a large number of modes. Our results pave the way for the development of advanced multidimensional quantum technologies.

REFERENCES AND NOTES

- N. J. Cerf, M. Bourennane, A. Karlsson, N. Gisin, Security of quantum key distribution using d-level systems. *Phys. Rev. Lett.* **88**, 127902 (2002). [doi:10.1103/PhysRevLett.88.127902](https://doi.org/10.1103/PhysRevLett.88.127902) Medline
- F. Bouchard, R. Fickler, R. W. Boyd, E. Karimi, High-dimensional quantum cloning and applications to quantum hacking. *Sci. Adv.* **3**, e1601915 (2017). [doi:10.1126/sciadv.1601915](https://doi.org/10.1126/sciadv.1601915) Medline
- N. T. Islam, C. C. W. Lim, C. Cahall, J. Kim, D. J. Gauthier, Provably secure and high-rate quantum key distribution with time-bin qudits. *Sci. Adv.* **3**, e1701491 (2017). [doi:10.1126/sciadv.1701491](https://doi.org/10.1126/sciadv.1701491) Medline
- H. M. Wiseman, S. J. Jones, A. C. Doherty, Steering, entanglement, nonlocality, and the Einstein-Podolsky-Rosen paradox. *Phys. Rev. Lett.* **98**, 140402 (2007). [doi:10.1103/PhysRevLett.98.140402](https://doi.org/10.1103/PhysRevLett.98.140402) Medline
- D. Collins, N. Gisin, N. Linden, S. Massar, S. Popescu, Bell inequalities for arbitrarily high-dimensional systems. *Phys. Rev. Lett.* **88**, 040404 (2002). [doi:10.1103/PhysRevLett.88.040404](https://doi.org/10.1103/PhysRevLett.88.040404) Medline
- A. Salavrakos, R. Augusiak, J. Tura, P. Wittek, A. Acín, S. Pironio, Bell inequalities tailored to maximally entangled states. *Phys. Rev. Lett.* **119**, 040402 (2017). [doi:10.1103/PhysRevLett.119.040402](https://doi.org/10.1103/PhysRevLett.119.040402) Medline
- R. Kaltenbaek, J. Lavoie, B. Zeng, S. D. Bartlett, K. J. Resch, Optical one-way quantum computing with a simulated valence-bond solid. *Nat. Phys.* **6**, 850–854 (2010). [doi:10.1038/nphys1777](https://doi.org/10.1038/nphys1777)
- M. Neeley, M. Ansmann, R. C. Bialczak, M. Hofheinz, E. Lucero, A. D. O’Connell, D. Sank, H. Wang, J. Wenner, A. N. Cleland, M. R. Geller, J. M. Martinis, Emulation of a quantum spin with a superconducting phase qudit. *Science* **325**, 722–725 (2009). [doi:10.1126/science.1173440](https://doi.org/10.1126/science.1173440) Medline
- B. P. Lanyon, M. Barbieri, M. P. Almeida, T. Jennewein, T. C. Ralph, K. J. Resch, G. J. Pryde, J. L. O’Brien, A. Gilchrist, A. G. White, Simplifying quantum logic using higher-dimensional Hilbert spaces. *Nat. Phys.* **5**, 134–140 (2009). [doi:10.1038/nphys1150](https://doi.org/10.1038/nphys1150)
- A. Bocharov, M. Roetteler, K. M. Svore, Factoring with qutrits: Shor’s algorithm on ternary and metaplectic quantum architectures. *Phys. Rev. A* **96**, 012306 (2017). [doi:10.1103/PhysRevA.96.012306](https://doi.org/10.1103/PhysRevA.96.012306)
- A. Mair, A. Vaziri, G. Weihs, A. Zeilinger, Entanglement of the orbital angular momentum states of photons. *Nature* **412**, 313–316 (2001). [doi:10.1038/35085529](https://doi.org/10.1038/35085529) Medline
- A. C. Dada, J. Leach, G. S. Buller, M. J. Padgett, E. Andersson, Experimental high-dimensional two-photon entanglement and violations of generalized Bell inequalities. *Nat. Phys.* **7**, 677–680 (2011). [doi:10.1038/nphys1996](https://doi.org/10.1038/nphys1996)
- E. Svetitsky, H. Suchowski, R. Resh, Y. Shalibo, J. M. Martinis, N. Katz, Hidden two-qubit dynamics of a four-level Josephson circuit. *Nat. Commun.* **5**, 5617 (2014). [doi:10.1038/ncomms6617](https://doi.org/10.1038/ncomms6617) Medline
- C. Senko, P. Richerme, J. Smith, A. Lee, I. Cohen, A. Retzker, C. Monroe, Quantum integer-spin chain with controllable interactions. *Phys. Rev. X* **5**, 021026 (2015). [doi:10.1103/PhysRevX.5.021026](https://doi.org/10.1103/PhysRevX.5.021026)
- S. Choi, N. Y. Yao, M. D. Lukin, Dynamical engineering of interactions in qudit ensembles. *Phys. Rev. Lett.* **119**, 183603 (2017). [doi:10.1103/PhysRevLett.119.183603](https://doi.org/10.1103/PhysRevLett.119.183603) Medline
- A. Martin, T. Guerreiro, A. Tiranov, S. Designolle, F. Fröwis, N. Brunner, M. Huber, N. Gisin, Quantifying photonic high-dimensional entanglement. *Phys. Rev. Lett.* **118**, 110501 (2017). [doi:10.1103/PhysRevLett.118.110501](https://doi.org/10.1103/PhysRevLett.118.110501) Medline
- Z. Xie, T. Zhong, S. Shrestha, X. A. Xu, J. Liang, Y.-X. Gong, J. C. Bienfang, A. Restelli, J. H. Shapiro, F. N. C. Wong, C. Wei Wong, Harnessing high-dimensional hyperentanglement through a biphoton frequency comb. *Nat. Photonics* **9**, 536–542 (2015). [doi:10.1038/nphoton.2015.110](https://doi.org/10.1038/nphoton.2015.110)
- M. Kues, C. Reimer, P. Roztocki, L. R. Cortés, S. Sciara, B. Wetzel, Y. Zhang, A. Cino, S. T. Chu, B. E. Little, D. J. Moss, L. Caspani, J. Azaña, R. Morandotti, On-chip generation of high-dimensional entangled quantum states and their coherent control. *Nature* **546**, 622–626 (2017). [doi:10.1038/nature22986](https://doi.org/10.1038/nature22986) Medline
- M. Malik, M. Erhard, M. Huber, M. Krenn, R. Fickler, A. Zeilinger, Multi-photon entanglement in high dimensions. *Nat. Photonics* **10**, 248–252 (2016). [doi:10.1038/nphoton.2016.12](https://doi.org/10.1038/nphoton.2016.12)
- R. Fickler, R. Lapkiewicz, W. N. Plick, M. Krenn, C. Schaeff, S. Ramelow, A. Zeilinger, Quantum entanglement of high angular momenta. *Science* **338**, 640–643 (2012). [doi:10.1126/science.1227193](https://doi.org/10.1126/science.1227193) Medline
- X. Cai, J. Wang, M. J. Strain, B. Johnson-Morris, J. Zhu, M. Sorel, J. L. O’Brien, M. G. Thompson, S. Yu, Integrated compact optical vortex beam emitters. *Science* **338**, 363–366 (2012). [doi:10.1126/science.1226528](https://doi.org/10.1126/science.1226528) Medline
- M. Reck, A. Zeilinger, H. J. Bernstein, P. Bertani, Experimental realization of any discrete unitary operator. *Phys. Rev. Lett.* **73**, 58–61 (1994). [doi:10.1103/PhysRevLett.73.58](https://doi.org/10.1103/PhysRevLett.73.58) Medline
- J. Carolan, C. Harrold, C. Sparrow, E. Martín-López, N. J. Russell, J. W. Silverstone, P. J. Shadbolt, N. Matsuda, M. Oguma, M. Itoh, G. D. Marshall, M. G. Thompson, J. C. F. Matthews, T. Hashimoto, J. L. O’Brien, A. Laing, Universal linear optics. *Science* **349**, 711–716 (2015). [doi:10.1126/science.aab3642](https://doi.org/10.1126/science.aab3642) Medline
- C. Schaeff, R. Polster, R. Lapkiewicz, R. Fickler, S. Ramelow, A. Zeilinger, Scalable fiber integrated source for higher-dimensional path-entangled photonic quNits. *Opt. Express* **20**, 16145 (2012). [doi:10.1364/OE.20.016145](https://doi.org/10.1364/OE.20.016145)
- R. Santagati, J. Wang, A. A. Gentile, S. Paesani, N. Wiebe, J. R. McClean, S. Morley-Short, P. J. Shadbolt, D. Bonneau, J. W. Silverstone, D. P. Tew, X. Zhou, J. L. O’Brien, M. G. Thompson, Witnessing eigenstates for quantum simulation of Hamiltonian spectra. *Sci. Adv.* **4**, eaap9646 (2018). [doi:10.1126/sciadv.aap9646](https://doi.org/10.1126/sciadv.aap9646) Medline
- D. Bonneau, J. W. Silverstone, M. G. Thompson, *Silicon Quantum Photonics* (Springer, 2016), pp. 41–82.
- J. Wang, S. Paesani, R. Santagati, S. Knauer, A. A. Gentile, N. Wiebe, M. Petruzzella, J. L. O’Brien, J. G. Rarity, A. Laing, M. G. Thompson, Experimental quantum Hamiltonian learning. *Nat. Phys.* **13**, 551–555 (2017). [doi:10.1038/nphys4074](https://doi.org/10.1038/nphys4074)
- N. C. Harris, G. R. Steinbrecher, M. Prabhu, Y. Lahini, J. Mower, D. Bunandar, C. Chen, F. N. C. Wong, T. Baehr-Jones, M. Hochberg, S. Lloyd, D. Englund, Quantum transport simulations in a programmable nanophotonic processor. *Nat. Photonics* **11**, 447–452 (2017). [doi:10.1038/nphoton.2017.95](https://doi.org/10.1038/nphoton.2017.95)
- See supplementary materials.
- M. Agnew, J. Leach, M. McLaren, F. S. Roux, R. W. Boyd, Tomography of the quantum state of photons entangled in high dimensions. *Phys. Rev. A* **84**, 062101 (2011). [doi:10.1103/PhysRevA.84.062101](https://doi.org/10.1103/PhysRevA.84.062101)
- D. Gross, Y.-K. Liu, S. T. Flammia, S. Becker, J. Eisert, Quantum state tomography via compressed sensing. *Phys. Rev. Lett.* **105**, 150401 (2010). [doi:10.1103/PhysRevLett.105.150401](https://doi.org/10.1103/PhysRevLett.105.150401) Medline
- E. Bolduc, G. Gariepy, J. Leach, Direct measurement of large-scale quantum

- states via expectation values of non-Hermitian matrices. *Nat. Commun.* **7**, 10439 (2016). doi:10.1038/ncomms10439 Medline
33. C. A. Riofrío, D. Gross, S. T. Flammia, T. Monz, D. Nigg, R. Blatt, J. Eisert, Experimental quantum compressed sensing for a seven-qubit system. *Nat. Commun.* **8**, 15305 (2017). doi:10.1038/ncomms15305 Medline
34. M. Navascués, T. Vértesi, Bounding the set of finite dimensional quantum correlations. *Phys. Rev. Lett.* **115**, 020501 (2015). doi:10.1103/PhysRevLett.115.020501 Medline
35. J. Sikora, A. Varvitsiotis, Z. Wei, Minimum dimension of a Hilbert space needed to generate a quantum correlation. *Phys. Rev. Lett.* **117**, 060401 (2016). doi:10.1103/PhysRevLett.117.060401 Medline
36. N. D. Mermin, Simple unified form for the major no-hidden-variables theorems. *Phys. Rev. Lett.* **65**, 3373–3376 (1990). doi:10.1103/PhysRevLett.65.3373 Medline
37. D. Mayers, A. Yao, in *39th Annual Symposium on Foundations of Computer Science (FOCS)* (1998), p. 503.
38. A. Coladangelo, K. T. Goh, V. Scarani, All pure bipartite entangled states can be self-tested. *Nat. Commun.* **8**, 15485 (2017). doi:10.1038/ncomms15485 Medline
39. T. H. Yang, T. Vértesi, J.-D. Bancal, V. Scarani, M. Navascués, Robust and versatile black-box certification of quantum devices. *Phys. Rev. Lett.* **113**, 040401 (2014). doi:10.1103/PhysRevLett.113.040401 Medline
40. M. Herrero-Collantes, J. C. Garcia-Escartin, Quantum random number generators. *Rev. Mod. Phys.* **89**, 015004 (2017). doi:10.1103/RevModPhys.89.015004
41. S. Pironio, A. Acín, S. Massar, A. B. de la Giroday, D. N. Matsukevich, P. Maunz, S. Olmschenk, D. Hayes, L. Luo, T. A. Manning, C. Monroe, Random numbers certified by Bell's theorem. *Nature* **464**, 1021–1024 (2010). doi:10.1038/nature09008 Medline
42. E. Passaro, D. Cavalcanti, P. Skrzypczyk, A. Acín, Optimal randomness certification in the quantum steering and prepare-and-measure scenarios. *New J. Phys.* **17**, 113010 (2015). doi:10.1088/1367-2630/17/11/113010
43. A. Acín, S. Pironio, T. Vértesi, P. Wittek, Optimal randomness certification from one entangled bit. *Phys. Rev. A* **93**, 040102 (2016). doi:10.1103/PhysRevA.93.040102
44. F. J. Curchod, M. Johansson, R. Augusiak, M. J. Hoban, P. Wittek, A. Acín, Unbounded randomness certification using sequences of measurements. *Phys. Rev. A* **95**, 020102 (2017). doi:10.1103/PhysRevA.95.020102
45. Y. Ding, D. Bacco, K. Dalgaard, X. Cai, X. Zhou, K. Rottwitt, L. K. Oxenløwe, High-dimensional quantum key distribution based on multicore fiber using silicon photonic integrated circuits. *npj Quantum Inform.* **3**, 25 (2017). doi:10.1038/s41534-017-0026-2
46. R. Fickler, R. Lapkiewicz, M. Huber, M. P. J. Lavery, M. J. Padgett, A. Zeilinger, Interface between path and orbital angular momentum entanglement for high-dimensional photonic quantum information. *Nat. Commun.* **5**, 4502 (2014). doi:10.1038/ncomms5502 Medline
47. A. Laing, V. Scarani, J. G. Rarity, J. L. O'Brien, Reference frame-independent quantum key distribution. *Phys. Rev. A* **82**, 012304 (2010). doi:10.1103/PhysRevA.82.012304
48. Y. Ding, C. Peucheret, H. Ou, K. Yvind, Fully etched apodized grating coupler on the SOI platform with -0.58 dB coupling efficiency. *Opt. Lett.* **39**, 5348–5350 (2014). doi:10.1364/OL.39.005348 Medline
49. A. E.-J. Lim, J. Song, Q. Fang, C. Li, X. Tu, N. Duan, K. K. Chen, R. P.-C. Tern, T.-Y. Liow, Review of silicon photonics foundry efforts. *IEEE J. Sel. Top. Quantum Electron.* **20**, 405–416 (2013). doi:10.1109/JSTQE.2013.2293274
50. S. K. Selvaraja, P. De Heyn, G. Winroth, P. Ong, G. Lepage, C. Cailler, A. Rigny, K. Bourdelle, W. Bogaerts, D. VanThourhout, J. Van Campenhout, P. Absil, Highly uniform and low-loss passive silicon photonics devices using a 300mm CMOS platform. In *Optical Fiber Communication Conference* (2014), paper Th2A.33. doi:10.1364/OFC.2014.Th2A.33
51. J. W. Silverstone, D. Bonneau, K. Ohira, N. Suzuki, H. Yoshida, N. Iizuka, M. Ezaki, C. M. Natarajan, M. G. Tanner, R. H. Hadfield, V. Zwiller, G. D. Marshall, J. G. Rarity, J. L. O'Brien, M. G. Thompson, On-chip quantum interference between silicon photon-pair sources. *Nat. Photonics* **8**, 104–108 (2013). doi:10.1038/nphoton.2013.339
52. W. R. Clements, P. C. Humphreys, B. J. Metcalf, W. S. Kolthammer, I. A. Walmsley, Optimal design for universal multiport interferometers. *Optica* **3**, 1460 (2016). doi:10.1364/OPTICA.3.001460
53. O. Kahl, S. Ferrari, V. Kovalyuk, A. Vetter, G. Lewes-Malandrakis, C. Nebel, A. Korneev, G. Goltsman, W. Pernice, Spectrally multiplexed single-photon detection with hybrid superconducting nanophotonic circuits. *Optica* **4**, 557 (2017). doi:10.1364/OPTICA.4.000557
54. S. Paesani, A. A. Gentile, R. Santagati, J. Wang, N. Wiebe, D. P. Tew, J. L. O'Brien, M. G. Thompson, Experimental Bayesian quantum phase estimation on a silicon photonic chip. *Phys. Rev. Lett.* **118**, 100503 (2017). doi:10.1103/PhysRevLett.118.100503 Medline
55. D. Gross, Recovering low-rank matrices from few coefficients in any basis. *IEEE Trans. Inf. Theory* **57**, 1548–1566 (2011). doi:10.1109/TIT.2011.2104999
56. S. T. Flammia, D. Gross, Y.-K. Liu, J. Eisert, Quantum tomography via compressed sensing: Error bounds, sample complexity, and efficient estimators. *New J. Phys.* **14**, 095022 (2012). doi:10.1088/1367-2630/14/9/095022
57. J. Löfberg, YALMIP: a toolbox for modeling and optimization in MATLAB. In *2004 IEEE International Symposium on Computer Aided Control Systems Design (CACSD)* (2004). doi:10.1109/CACSD.2004.1393890
58. J. Sturm, Using SeDuMi 1.02, A Matlab toolbox for optimization over symmetric cones. *Optim. Methods Softw.* **11**, 625–653 (1999). doi:10.1080/10556789908805766
59. A. Peres, Incompatible results of quantum measurements. *Phys. Lett. A* **151**, 107–108 (1990). doi:10.1016/0375-9601(90)90172-K
60. P. Aravind, Bell's theorem without inequalities and only two distant observers. *Found. Phys. Lett.* **15**, 397–405 (2002).
61. M. Navascués, S. Pironio, A. Acín, Bounding the set of quantum correlations. *Phys. Rev. Lett.* **98**, 010401 (2007). doi:10.1103/PhysRevLett.98.010401 Medline
62. A. Acín, T. Durt, N. Gisin, J. I. Latorre, Quantum nonlocality in two three-level systems. *Phys. Rev. A* **65**, 052325 (2002). doi:10.1103/PhysRevA.65.052325
63. D. Cavalcanti, P. Skrzypczyk, Quantum steering: A review with focus on semidefinite programming. *Rep. Prog. Phys.* **80**, 024001 (2017). doi:10.1088/1361-6633/80/2/024001 Medline
64. V. Scarani, H. Bechmann-Pasquinucci, N. J. Cerf, M. Dušek, N. Lütkenhaus, M. Peev, The security of practical quantum key distribution. *Rev. Mod. Phys.* **81**, 1301–1350 (2009). doi:10.1103/RevModPhys.81.1301

ACKNOWLEDGMENTS

We acknowledge A.C. Dada, P.J. Shadbolt, J. Carolan, C. Sparrow, W. McCutcheon, A.A. Gentile, D.A.B. Miller and Q. He for useful discussions. We thank W.A. Murray, M. Louit and R. Collins for experimental assistance. **Funding:** we acknowledge the support from the Engineering and Physical Sciences Research Council (EPSRC), European Research Council (ERC), and European Commission (EC), including PICQUE, BBOI, QuChip, QITBOX, and the Center of Excellence, Denmark SPOC (ref DNRF123), Bristol NSQI. J.W. acknowledges the Chinese National Young 1000 Tal-

ents Plan. P.K. is supported by the Royal Society through a University Research Fellowship (UHNL). L. M. is supported by the Villum Fonden via the QMATH Centre of Excellence (No. 10059) and also acknowledges the support from the EPSRC (EP/L021005/1). We also acknowledge support from the Spanish MINECO (QIBEQI FIS2016-80773-P and Severo Ochoa SEV-2015-0522), the Fundacio Cellex, the Generalitat de Catalunya (SGR875 and CERCA Program), and the AXA Chair in Quantum Information Science. This project has received funding from the European Union's Horizon 2020 research and innovation program under the Marie Skłodowska-Curie grant agreements No. 705109, 748549, and 609405. Q.G. acknowledges the National Key R and D Program of China (no.2013CB328704). J.L.O. acknowledges a Royal Society Wolfson Merit Award and a Royal Academy of Engineering Chair in Emerging Technologies. Fellowship support from EPSRC is acknowledged by A.L. (EP/N003470/1). M.G.T. acknowledges support from the ERC starter grant (ERC-2014-STG 640079) and an EPSRC Early Career Fellowship (EP/K033085/1). **Author contributions:** J.W., S.P. and Y.D. contributed equally to this work. J.W. designed the experiment. Y.D. designed and fabricated the device. J.W., S.P., Y.D., R.S. and J.W.S. built the setup and carried out the experiment. S.P., P.S., A.S., J.T., R.A., L.M., D.B. and D.Bonneau performed the theoretical analysis. Q.G., A.A., K.R., L.K.O., J.L.O., A.L and M.G.T. managed the project. All authors discussed the results and contributed to the manuscript. **Competing interests:** All authors declare no competing final interests. **Data and materials availability:** All data are available in the manuscript or in the supplementary materials.

SUPPLEMENTARY MATERIALS

www.scienmag.org/cgi/content/full/science.aar7053/DC1

Materials and Methods

Figs. S1 to S7

Tables S1 to S9

References (48–64)

8 December 2017; accepted 27 February 2018

Published online 8 March 2018

10.1126/science.aar7053

Table 1. Experimental values for multidimensional CGLMP Bell correlations. Measured CGLMP values are given with experimental errors. Values in (*) refer to the LHV classical bound; those in {*} refer to theoretical bounds for d -dimensional maximally entangled states. Errors are given by photon Poissonian noise.

Dim	CGLMP S_d
2	(2) $2.810 \pm 0.014 \{2.828\}$
3	(2) $2.845 \pm 0.012 \{2.873\}$
4	(2) $2.867 \pm 0.014 \{2.896\}$
5	(2) $2.763 \pm 0.014 \{2.910\}$
6	(2) $2.629 \pm 0.010 \{2.920\}$
7	(2) $2.532 \pm 0.013 \{2.927\}$
8	(2) $2.650 \pm 0.012 \{2.932\}$

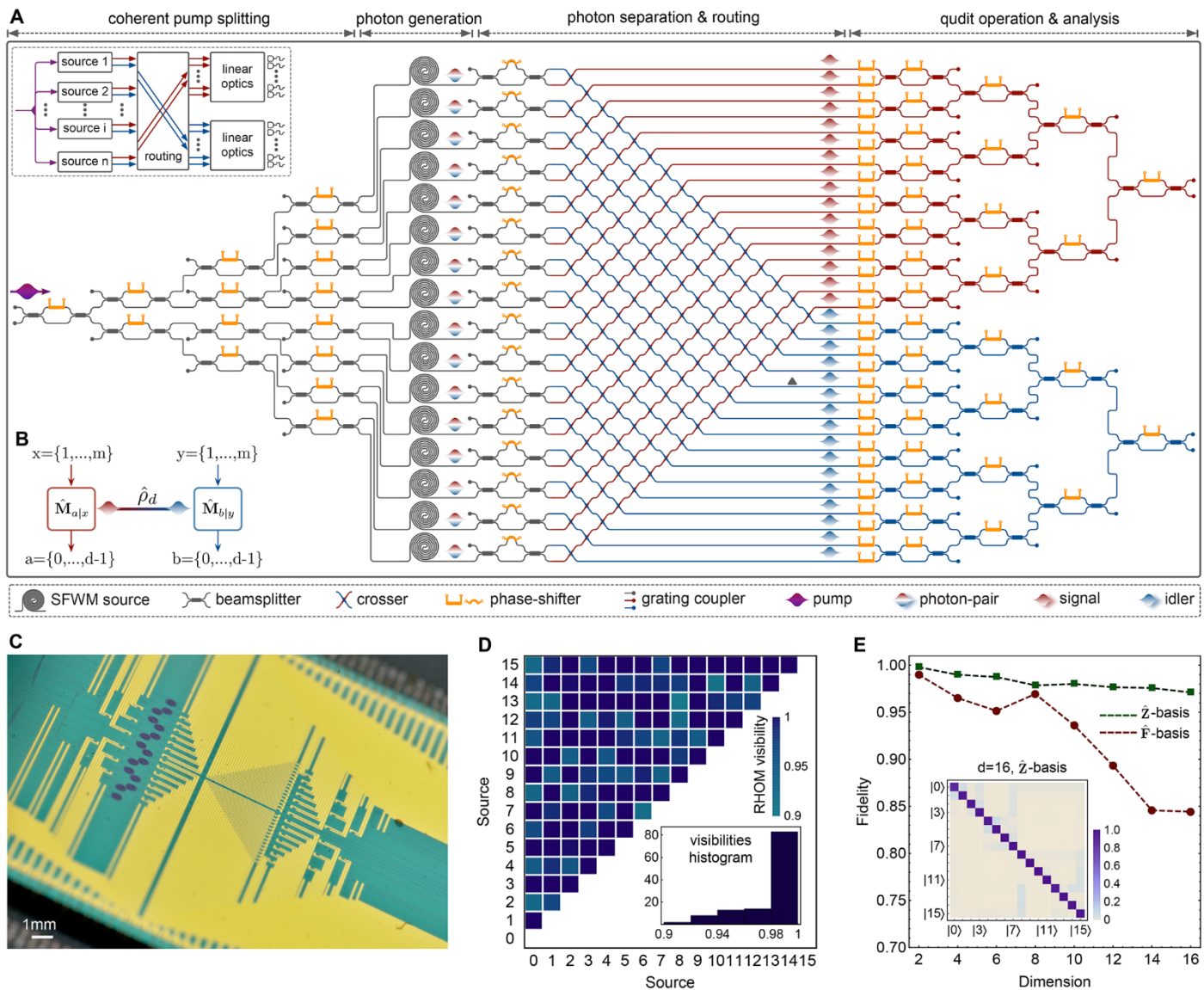


Fig. 1. Diagram and characterization of the multidimensional silicon quantum photonic circuit. (A) Circuit diagram. The device monolithically integrates 16 SFWM photon-pair sources, 93 thermo-optical phase-shifters, 122 multimode interferometers (MMI) beamsplitter, 256 waveguide-crossers and 64 optical grating couplers. A photon pair is generated by SFWM in superposition across 16 optical modes, producing a tunable multidimensional bipartite entangled state. The two photons, signal and idler, are separated by an array of asymmetric MZI filters and routed by a network of crossers, allowing the local manipulation of the state by linear-optical circuits. Using triangular networks of MZIs, we perform arbitrary local projective measurements. The photons are coupled off the chip into fibers using grating couplers, and detected by two superconducting nanowire detectors. The inset represents a general schematic for universal generation and manipulation of bipartite multidimensional entangled states. (B) Framework for correlation measurements on a shared d -dimensional state $\hat{\rho}_d$. $\hat{M}_{a|x}$ and $\hat{M}_{b|y}$ represent the operators associated to local measurements x on Alice and y on Bob, with outcomes a and b respectively. (C) Photograph of the device. Silicon waveguides and 16 SFWM sources can be observed as black lines. Gold wires allow the electronic access of each phase-shifter. (D) Visibilities for the two-photon RHOM experiments to test sources' indistinguishability. The inset shows the histogram of all 120 measured visibilities, with a mean value of 0.984 ± 0.025 . (E) Statistical fidelity for d -dimensional projectors, in both the computational \hat{Z} -basis and the Fourier \hat{F} -basis. The inset shows the measured distribution for the 16-dimensional projector in the \hat{Z} -basis.

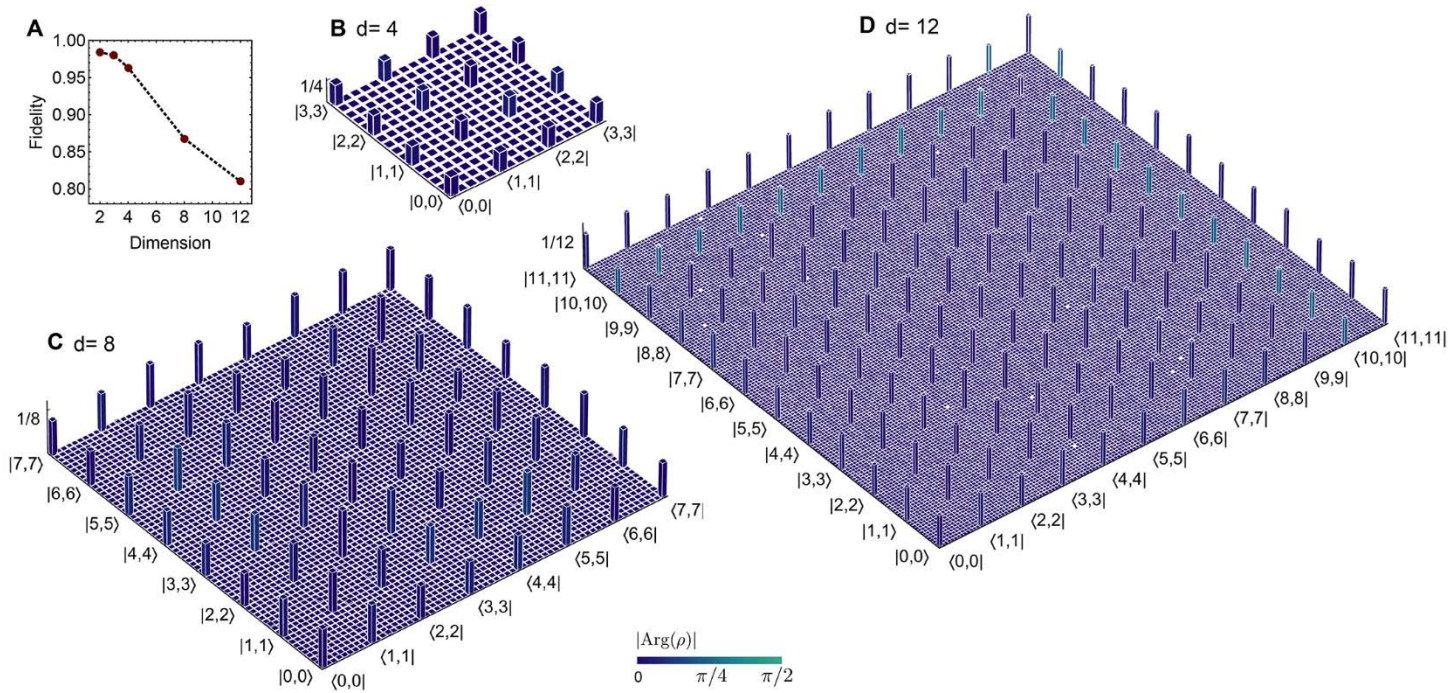


Fig. 2. Experimental quantum state tomographies. (A) Measured quantum fidelities $\langle \psi_d^+ | \hat{\rho}_d | \psi_d^+ \rangle$, where $\hat{\rho}_d$ represents the reconstructed states and $|\psi_d^+\rangle$ refers to the ideal d -dimensional maximally entangled state. Reconstructed density matrices for the entangled states in dimension (B) 4, (C) 8, and (D) 12 using compressed sensing techniques. Column heights represent the absolute values $|\rho|$ while colors represent the phases $|\text{Arg}(\rho)|$. The phase information for matrix elements with module $|\rho_{ij}| < 0.01$ is approximately randomly distributed and not displayed for more clarity.

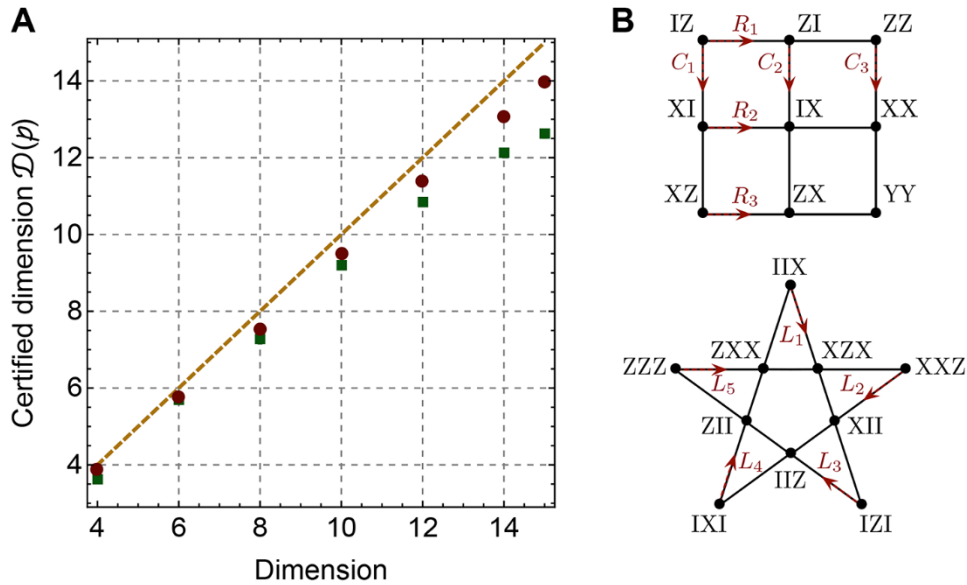


Fig. 3. Verification of system dimensionality. (A) Experimental results. Data points refer to the measured lower bounds on the local dimension of the generated entangled states; green (red) points represent data for the measurement scenario I (II). The yellow line refers to ideal values. Errors are smaller than the markers and neglected in the plot for clarity. (B) Correlation measurements associated to optimal strategies for Magic Square and Pentagram games. X , Y and Z are Pauli operators and I is the identity. Red lines C_i , R_i and L_i are associated to different measurement settings. Single Magic Square game, Magic Pentagram game, and two copies of the Magic Square game are used in an attempt to certify the dimension for states with local dimension $d = 4$, $d = 6, 8$, and $d = 10, 12, 14, 15$, respectively. The correct dimension is certified for up to $d = 10$ when using measurement scenario I and up to $d = 14$ when using scenario II.

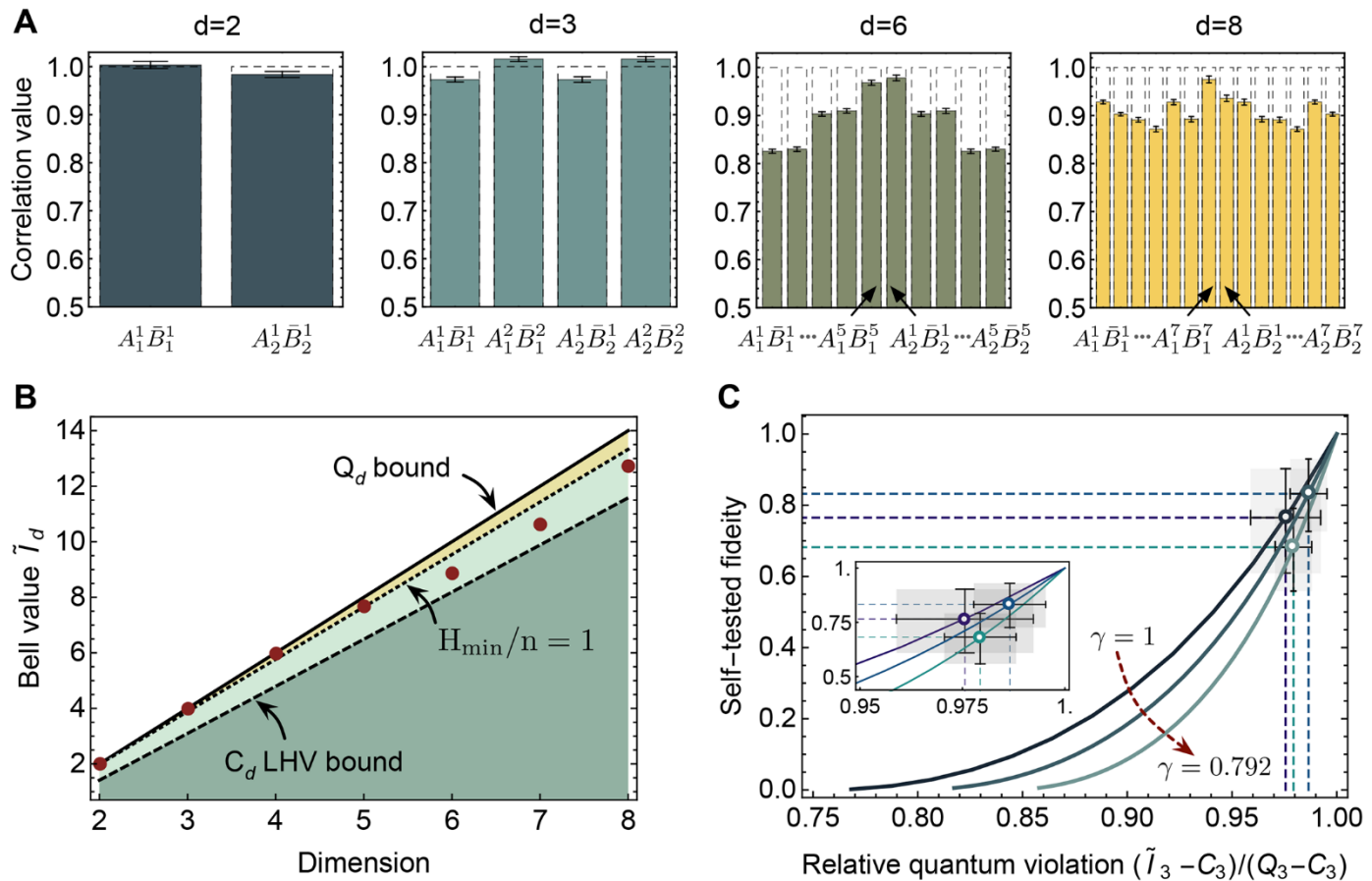


Fig. 4. Bell violation and self-testing on multidimensional entangled states. (A) Measured values of the $2(d-1)$ correlators $\text{Re}\left[\langle A_i^l \bar{B}_i^l \rangle\right]$. Dashed boxes refer to theoretical values. (B) Violation of the generalized SATWAP Bell-type inequalities for d -dimensional states. Red points are experimentally measured \tilde{I}_d values. Bell inequalities of the form $\tilde{I}_d \leq C_d$ are here violated, where C_d is the classical LHV bound (dashed line). The Tsirelson bound Q_d (solid line) represents the maximal violation for quantum systems. The dotted line represents the threshold above which more than 1 random bit can be extracted per output symbol from Bell correlations. (C) DI self-testing of entangled qutrit states $(|00\rangle + \gamma|11\rangle + |22\rangle)/\sqrt{2+\gamma^2}$ for $\gamma = 1, 0.9, 0.792$. Self-tested lower bounds on the fidelities to ideal states are plotted as a function of the relative violation for more clarity. The significant uncertainty on the fidelity value is due to the general limited robustness of self-testing protocols. All errors are estimated from photon Poissonian statistics, and those in (B) are smaller than markers.

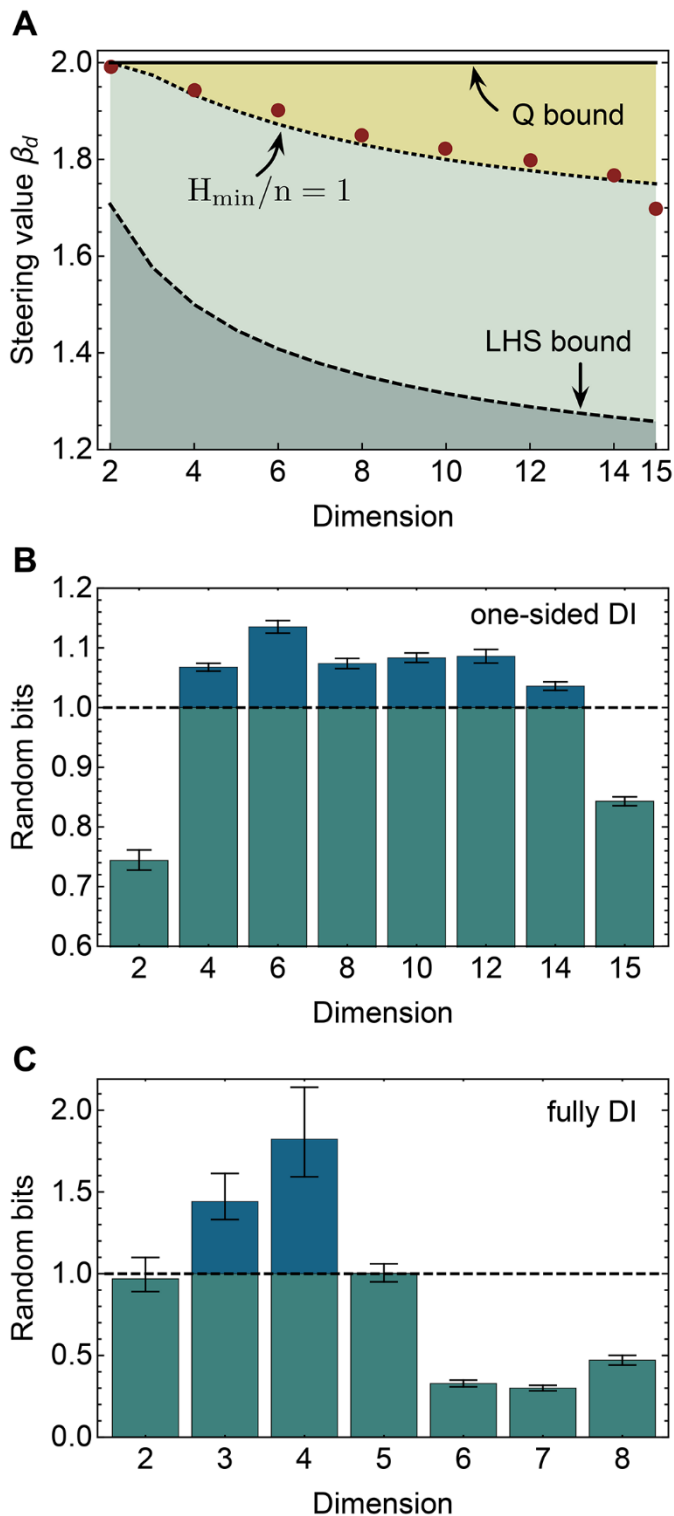


Fig. 5. Certification of multidimensional randomness expansion. (A) Multidimensional EPR steering is certified by violating the inequality $\beta_d \leq 1 + 1/\sqrt{d}$ (dashed line). Red points are experimentally measured steering values β_d . The dotted line denotes the threshold above which more than 1 random bit is generated per round from steering correlations. (B) Randomness per round certified in a one-sided DI scenario by d -dimensional steering correlations. (C) Randomness per round certified in a fully DI scenario by d -dimensional Bell correlations. Above the dashed line in (B) and (C), more than 1 private random bits are generated per round. Error bars are given by Poissonian statistics, and those in (A) are smaller than markers.

Multidimensional quantum entanglement with large-scale integrated optics

Jianwei Wang, Stefano Paesani, Yunhong Ding, Raffaele Santagati, Paul Skrzypczyk, Alexia Salavrakos, Jordi Tura, Remigiusz Augusiak, Laura Mancinska, Davide Bacco, Damien Bonneau, Joshua W. Silverstone, Qihuang Gong, Antonio Acín, Karsten Rottwitt, Leif K. Oxenløwe, Jeremy L. O'Brien, Anthony Laing and Mark G. Thompson

published online March 8, 2018

ARTICLE TOOLS

<http://science.scienmag.org/content/early/2018/03/07/science.aar7053>

SUPPLEMENTARY MATERIALS

<http://science.scienmag.org/content/suppl/2018/03/07/science.aar7053.DC1>

REFERENCES

This article cites 60 articles, 7 of which you can access for free

<http://science.scienmag.org/content/early/2018/03/07/science.aar7053#BIBL>

PERMISSIONS

<http://www.scienmag.org/help/reprints-and-permissions>

Use of this article is subject to the [Terms of Service](#)